INTERFACE FOCUS

rsfs.royalsocietypublishing.org

Research

Cite this article: Barrera G, Serpe L, Celegato F, Coïsson M, Martina K, Canaparo R, Tiberto P. 2016 Surface modification and cellular uptake evaluation of Au-coated $Ni_{80}Fe_{20}$ nanodiscs for biomedical applications. *Interface Focus* **6**: 20160052.
http://dx.doi.org/10.1098/rsfs.2016.0052

One contribution of 12 to a theme issue 'Multifunctional nanostructures for diagnosis and therapy of diseases'.

Subject Areas:
biomaterials, biotechnology, nanotechnology

Keywords:
self-assembly, magnetic nanodiscs, magnetization reversal, cytoxicity

Author for correspondence:
Paola Tiberto
e-mail: p.tiberto@inrim.it

THE ROYAL SOCIETY PUBLISHING

Surface modification and cellular uptake evaluation of Au-coated $Ni_{80}Fe_{20}$ nanodiscs for biomedical applications

Gabriele Barrera[1], Loredana Serpe[2], Federica Celegato[1], Marco Coïsson[1], Katia Martina[2], Roberto Canaparo[2] and Paola Tiberto[1]

[1]Nanoscience and Material Division, INRiM, 10135 Torino, Italy
[2]Department of Drug Science and Technology, University of Turin, 10125 Torino, Italy

GB, 0000-0002-3174-8092

A nanofabrication technique based on self-assembling of polystyrene nanospheres is used to obtain magnetic $Ni_{80}Fe_{20}$ nanoparticles with a disc shape. The free-standing nanodiscs (NDs) have diameter and thickness of about 630 nm and 30 nm, respectively. The versatility of fabrication technique allows one to cover the ND surface with a protective gold layer with a thickness of about 5 nm. Magnetization reversal has been studied by room-temperature hysteresis loop measurements in water-dispersed free-standing NDs. The reversal shows zero remanence, high susceptibility and nucleation/annihilation fields due to spin vortex formation. In order to investigate their potential use in biomedical applications, the effect of NDs coated with or without the protective gold layer on cell growth has been evaluated. A successful attempt to bind cysteine-fluorescein isothiocyanate (FITC) derivative to the gold surface of magnetic NDs has been exploited to verify the intracellular uptake of the NDs by cytofluorimetric analysis using the FITC conjugate.

1. Introduction

In the last few years, magnetic nanoparticles have been widely studied to be exploited in biomedicine with different purposes [1,2]. However, recent developments in this field have brought an increased interest in the synthesis and characterization of new types of magnetic nanoparticles. In particular, the ability to control size, shape and composition of magnetic nanoparticles can provide flexibility for biomedical applications, such as DNA separation, cell labelling, magnetic resonance imaging, drug delivery and magnetic hyperthermia [3–6].

Magnetic nanoparticles require a surface treatment or coating to be exploited in biomedical applications to protect them from oxidation or redissolution, to prevent the aggregation among nanoparticles, to increase their biocompatibility and their affinity for other molecules to further extend their functionalities [7,8].

The well-known optical properties, surface chemistry and biological reactivity of gold have made this element widely used as coating material for magnetic nanoparticles. Gold coating improves not only the stability of the magnetic particles, but also provides a useful surface to bind chemical and biological entities maintaining unaltered the magnetic behaviour of the particles [9]. However, the direct chemical coating of magnetic particles with gold is difficult, due to the dissimilar nature of the two surfaces; consequently nowadays different routes are investigated [10–13].

Usually, the conventional methods to synthesize magnetic nanoparticles are via chemical routes [14,15]. Despite that they are low-cost methods allowing one to synthesize high volumes of nanoparticles, their major drawback is the difficulty to obtain monodispersed dimensions leading to different and not easily predictable magnetic behaviour. To overcome such limits, recent studies have demonstrated the viability to use top-down approaches to fabricate specifically designed magnetic nanoparticles [16–18].

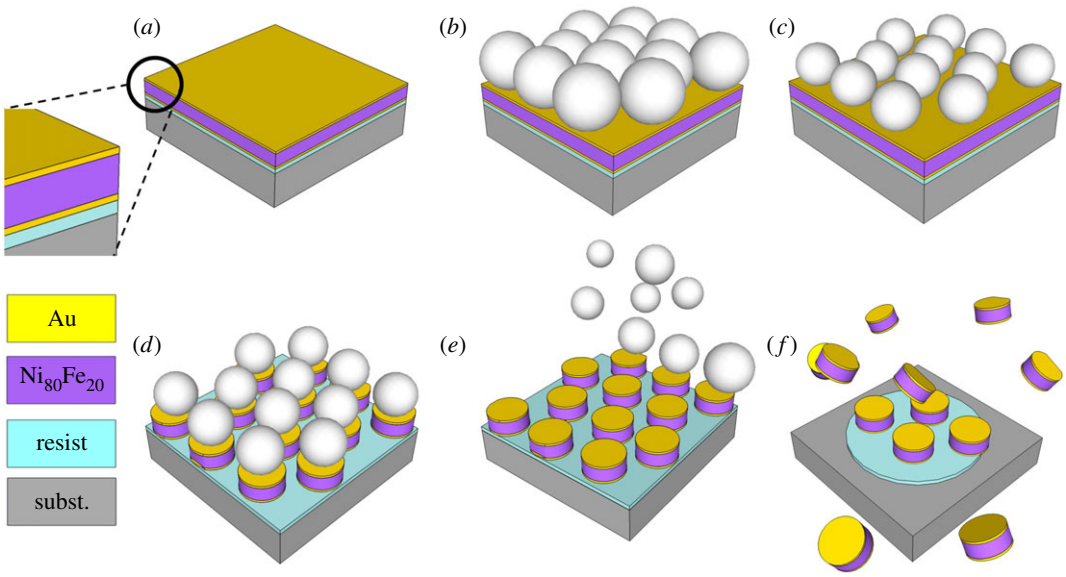

Figure 1. Schematic of the nanofabrication process: (*a*) sputter deposition of an Au/$Ni_{80}Fe_{20}$/Au tri-layer (thickness 5/30/5 nm); (*b*) deposition of a monolayer of polystyrene nanospheres (starting diameter 800 nm); (*c*) plasma etching in Ar to reduce PN diameter; (*d*) sputter etching to remove tri-layer among spheres; (*e*) sphere removal by sonication; and (*f*) chemical dissolution of resist underlayer resulting in disc detachment from the substrate.

In this work, magnetic $Ni_{80}Fe_{20}$ nanoparticles having disc shape have been synthesized and directly coated by a gold layer by means of a bottom-up self-assembling nanolithography process assisted by polystyrene nanospheres (PNs), which is widely considered as a valid alternative to conventional lithographic techniques (i.e. optical and electron) [19,20].

Nanoparticles having disc shape offer some advantages in biomedicine compared with the spherical ones; in particular, they adhere more effectively to the biological substrate [21], exhibit a higher margination propensity [22] and accumulate more efficiently in the organs [23]. Moreover, the nanodisc shape exhibits a larger surface available for functionalization with respect to spherical nanoparticles allowing the same biomedical results with a lower nanoparticle concentration reducing toxicity issues. These results indicate their potential use for the systemic delivery of drugs, in biomedical imaging and in hyperthermia treatments.

The magnetic $Ni_{80}Fe_{20}$ alloy and the size of nanodiscs (NDs) were chosen to induce a vortex-state spins arrangement in each nanostructure. This magnetic arrangement possesses the peculiar property of a zero remanence as in the case of superparamagnetic nanoparticles, but compared to them it has a higher magnetic saturation and susceptibility as well as the appearance of hysteresis at high fields [24]. In particular, high magnetic saturation and susceptibility allow one to reach a higher magnetization value at lower applied magnetic fields; therefore, they ensure an improvement in ND detection or manipulation using low fields. Such a feature together with a better vehiculation in blood vessels [22] allows the use of magnetic NDs for drug delivery application exploiting lower magnetic field gradient. Moreover, the hysteresis at high fields ensures a more efficient heat generation due to magnetic losses when the NDs are submitted to a radiofrequency field overcoming vortex expulsion field. For these reasons, these peculiar properties make the nanoparticles with magnetic vortex behaviour a promising candidate for diverse biomedical applications, especially in cancer cell detection and destruction by different means, including hyperthermia [6,25,26].

A thorough knowledge of the potential cytotoxicity and the interaction with cells of magnetic NDs is crucial for their biomedical applications [27]; therefore, a detailed study about the effects on cell viability is essential. In particular, in this paper, a comparative cytotoxicity study of Au-coated and bare $Ni_{80}Fe_{20}$ NDs at different concentrations has been performed on HT-29 human colorectal adenocarcinoma cells. Subsequently, a functionalization of gold surface of coated NDs was performed with a cysteine-fluorescein isothiocyanate (FITC) derivative in order to induce a random fluorescence and use them to evaluate the intracellular uptake.

2. Material and methods

2.1. Nanofabrication process of nanodiscs

Au-coated ferromagnetic nanodiscs (Au-NDs) are fabricated by exploiting PN lithography [16]. The multi-step process is schematized in figure 1 (note that is a not-to-scale scheme). In the first step, figure 1*a*, an Si substrate is coated by a layer of optical resist; on top of this an Au/$Ni_{80}Fe_{20}$/Au tri-layer film is sputtered each layer having thickness of 5 nm/30 nm/5 nm, respectively. The gold layer deposited by sputtering both before and after the magnetic material deposition has the purpose of coating the magnetic $Ni_{80}Fe_{20}$ core with biocompatible surface and for subsequent bio-functionalization. Then, an almost hexagonal-close-packed monolayer of PNs (starting diameter 800 nm) is deposited by floating technique onto the tri-layer, (as illustrated in figure 1*b*). In the third step, the PN diameter is reduced by plasma etching in Ar^+ in order to expose a portion of the tri-layer surface among PNs (figure 1*c*). In the present case, at this step, the etching time has been chosen in order to obtain the final PN diameter of about 630 nm. In the step shown in figure 1*d*, the PNs are used as a hard mask for sputter etching with Ar^+ ions used to remove the exposed tri-layer material among the PNs. The subsequent removal of the PN mask (lift-off) by sonication in deionized water leaves an array of ordered nanodots on the surface of the resist layer having the same composition and thickness as the starting continuous tri-layer film (figure 1*e*). In the last step of fabrication process, the underlayer of resist is dissolved in acetone and ends up with detached

free-standing Au-NDs (figure 1*f*) dispersed in the solvent. Through several rinsings with deionized water assisted by magnetic separation using a field gradient, the Au-NDs were cleaned by acetone and in the end dispersed in deionized water.

In order to evaluate the effect of Au layer, the same process has been used by depositing only the $Ni_{80}Fe_{20}$ film ($t = 30$ nm) in place of the tri-layer shown in figure 1*a*. In this case, the final sample is therefore constituted by bare $Ni_{80}Fe_{20}$ magnetic nanodiscs (bare-NDs) dispersed in water.

2.2. Morphological and magnetic characterization

Hysteresis loops at room temperature have been measured for bare or Au-coated NDs in water solution by using a vibrating sample magnetometer in the magnetic field range ± 1500 Oe. The Au-ND morphology was examined by scanning electron microscopy (SEM) instrument equipped with a scanning transmission electron microscopy (STEM) detector. A drop of the Au-NDs suspended in water has been placed on a standard copper grid, followed by drying.

2.3. Functionalization of nanodiscs with fluorescein isothiocyanate

In total, 2.5 mg of cysteine (0.015 mmol) and 3 mg of FITC (0.077 mmol) have been dissolved in 1 ml of DMSO/0.1 M phosphate-buffered saline (2 : 1) and left under shaking 4 h. Twenty-seven microlitres of the solution has been transferred and added to 1 ml of ND suspension (7.74×10^8 ea ml^{-1}) in 1 ml of DMSO/0.1 M phosphate-buffered saline (2 : 1) and incubated overnight. The final NDs/FITC have been washed two times with DMSO (1 ml^{-1}) and eight times with 0.1 M phosphate-buffered saline.

2.4. Biological assays

2.4.1. Cell line and culturing

The HT-29 human colorectal adenocarcinoma cell line (ATCC, Rockville, MD, USA) has been cultured in Eagle's minimum essential medium supplemented with 2 mM L-glutamine, 100 UI ml^{-1} penicillin, 100 µg ml^{-1} streptomycin and 10% fetal bovine serum (Sigma Aldrich, St Louis, MO, USA). Cell lines have been kept in a humidified atmosphere of 5% CO_2 air at 37°C.

The effect that NDs with and without the protective gold layer had on HT-29 cell growth has been evaluated using a WST-1 cell proliferation assay (Roche Applied Science, Penzberg, Germany). In total, 1.5×10^3 HT-29 cells have been seeded in 100 µl of growth medium in replicates ($n = 8$) in a 96-well culture plate. After 24 h of cell growth, the medium has been removed and the cells incubated with experimental media of differing ND concentrations (0.1, 1, 10 and 50 µg ml^{-1}). The WST-1 reagent (Roche Applied Science) (10/100 µl) has been added, at 24, 48 and 72 h, and plates have been incubated at 37°C in 5% CO_2 for 90 min. Well absorbance was measured at 450 and 620 nm (reference wavelength) in a microplate reader Asys UV340 (Biochrom, Cambridge, UK).

2.4.2. Flow cytometric analysis

Analysis of ND cellular uptake has been carried out on C6 flow cytometry equipment (Accuri Cytometers, Milano, Italy). Briefly, 1×10^5 cells have been plated in 6-well culture plates and incubated with FITC conjugated gold NDs (10 µg ml^{-1}) for 1, 8 and 24 h. Cells have been detached after each incubation period using a 0.05% trypsin–0.02% EDTA solution and re-suspended in 500 µl phosphate-buffered solution. They have been then run on the C6 flow cytometer, which considered 10 000 events, using 488 nm excitation to measure the intracellular NDs. Intracellular fluorescence is expressed as integrated median fluorescence intensity (iMFI). This is the product of the frequency of cells that are positive to FITC conjugated NDs and the median fluorescence intensity of the cells.

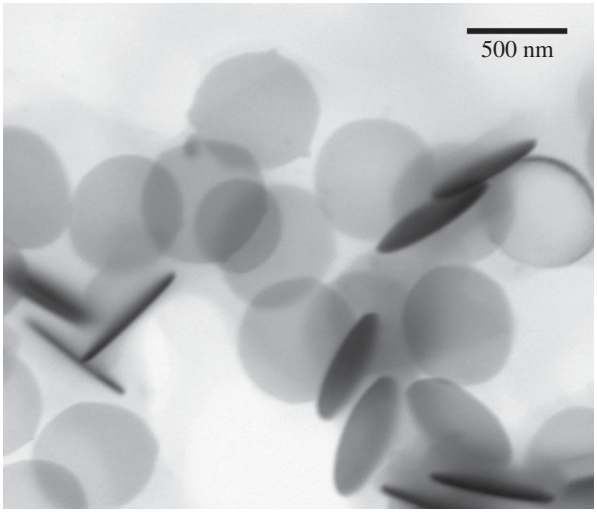

Figure 2. SEM image of free-standing Au-NDs placed on a standard copper grid.

3. Results and discussion

The nanosphere lithography used to synthetize the bare and Au-NDs (figure 1) comes out as an easy-to-use and low-cost method to nanostructure thin films. The major drawback of this technique is normally the lack of long-range order and the formation of some defects in the array in comparison with similar arrays obtained by means of optical or electron conventional lithographic processes [28]; however, in this context such limits are overcome by the fact that the final samples consist of free NDs detached from the substrate and dispersed in liquid solution (figure 1*f*). Therefore, the actual ordering of the NDs on the substrate has no relevance on the final product.

On the other hand, the nanosphere lithography offers higher resolution patterning than conventional optical techniques maintaining the same parallel writing method where the whole pattern is obtained simultaneously using the nanospheres as a hard mask dictating the features to be reproduced (figure 1*d*). Therefore, this parallel lithography process is fast and allows a wide surface coverage resulting in a promising, versatile and low-cost method for nanostructuring multilayer thin films producing ordered arrays of dots (figure 1*e*). Depending on the available experimental set-up, the final samples can be patterned by nanosphere lithography over surface areas from square millimetres to square centimetres [29].

In order to evaluate the packing density (η, fraction of surface area occupied by dots with respect to the whole substrate area) of the obtained dots array and consequently their area number density (ρ), some SEM images (with field of view of 37×32 µm^2) were taken in different regions of a sample having dots still attached on the substrate (as shown in figure 1*e*), resulting in $\eta = 0.62$ and $\rho = 1.2 \times 10^8$ dots cm^{-2}. Given the size of Si substrate used to fabricate both bare and Au-NDs samples is 2.54×2.54 cm^2, the total number of NDs in each sample is about of 7.74×10^8.

In addition, it is worth mentioning that this fabrication process does not allow a complete Au-coating of the $Ni_{80}Fe_{20}$ magnetic core because the lateral surface of the dots remains

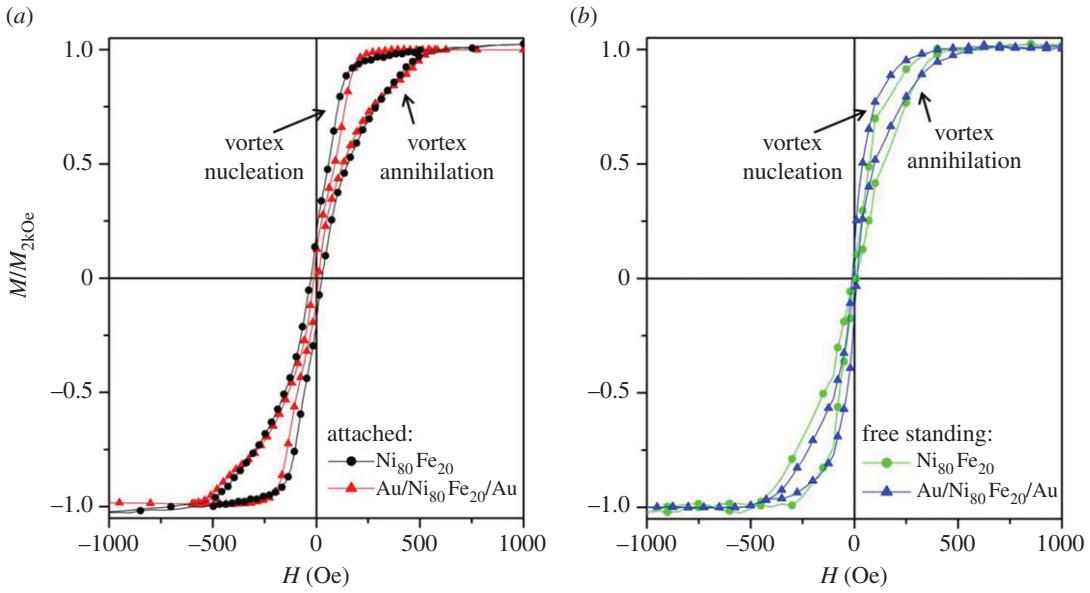

Figure 3. Room-temperature hysteresis loops of samples for: (*a*) NDs attached on Si substrate (black circles and red triangles for bare and Au-coated $Ni_{80}Fe_{20}$ NDs, respectively); (*b*) NDs dispersed in deionized water (green circles and blue triangles for bare and Au-coated $Ni_{80}Fe_{20}$ NDs, respectively).

uncovered, as shown in figure 1*f*, in particular only 91.5% of the total surface area of NDs is coated by the gold layer.

A drop of solution was placed on a standard copper grid in order to investigate the morphology of the as-fabricated Au-NDs by SEM equipped with the STEM detector (figure 2). As expected, a disc shape with a diameter of about 630 nm (coincident with the reduced diameter of PNs used as hard mask in the lithographic process) is observed. It is worth noting that the ND contour is well defined, not notched or damaged, indicating that the lithography assisted by PNs is a viable alternative to conventional ones (e.g. optical or electron).

The normalized room-temperature hysteresis loops measured both on bare and Au-coated $Ni_{80}Fe_{20}$NDs still attached on the substrate and subsequently dispersed in water are shown in figure 3. As expected, the magnetization reversal of bare-NDs (black and green circles, respectively, for attached (figure 3*a*) and water-dispersed (figure 3*b*) discs) is typical of a magnetic vortex behaviour [24,30]. The loops exhibit a magnetic remanence close to zero and an almost linear behaviour at low fields followed by an increase of hysteresis at fields preceding the magnetic saturation. In particular, the low-field reversible linear behaviour corresponds to the movement of magnetic vortex perpendicular to the applied field across the ND. Furthermore, increasing the field beyond a certain field value (annihilation field (H_{an})), the magnetic vortex gets annihilated and the magnetization reaches the saturation magnetization value M_s. Then, if the field is decreased from saturation, the magnetic vortex again nucleates at a field value (nucleation field (H_n)) lower than H_{an}. The difference between the nucleation field at decreasing field and annihilation field at increasing field is responsible for the occurrence of observed hysteresis. Reliable estimates of H_{an} and H_n values have been obtained as the field values at which maxima of the derivative of the magnetization curves appear ($H_n = 93$ Oe and $H_{an} = 420$ Oe for bare-NDs and $H_n = 120$ Oe and $H_{an} = 452$ Oe for Au-NDs). In samples constituted by NDs in water solution (figure 3*b*), the magnetization jumps corresponding to the annihilation and nucleation of the vortex are less marked than those measured in samples consisting of dots still attached to the substrate with in-plane applied field (figure 3*a*), preventing a precise estimation of H_n and H_{an} values. This smoothing of magnetization jump is due to the dispersion of NDs in water and the consequent random misalignment of their plane with respect to the applied magnetic field [16].

The magnetic vortex configuration is also observed in Au-NDs as indicated by the presence of nucleation and annihilation field in the hysteresis loops reported in figure 3 (red and blue triangles, respectively, for attached (figure 3*a*) and water-dispersed (figure 3*b*) discs). As expected, the gold layer does not substantially change the magnetic behaviour of the $Ni_{80}Fe_{20}$ magnetic core as both the annihilation and nucleation fields remain approximately unchanged.

To assess the cell viability, HT-29 cells have been exposed to varying concentrations of NDs with and without the protective gold layer (from 0.1 to 50 $\mu g\ ml^{-1}$) in order to investigate their cytotoxicity (figure 4). A dose-dependent increase in cytotoxicity has been observed after cell exposure to both ND formulations. However, lower cytotoxicity has been observed over time when cells were exposed to Au-NDs compared with bare-NDs: specifically 0.1 and 1 $\mu g\ ml^{-1}$ Au-NDs for up to 72 h, and 10 $\mu g\ ml^{-1}$ Au-NDs for up to 48 h, did not affect cell viability. Otherwise bare-NDs at 1 $\mu g\ ml^{-1}$ after 72 h exposure and 10 $\mu g\ ml^{-1}$ after 24 h exposure were cytotoxic. The highest ND concentration (50 $\mu g\ ml^{-1}$) was already cytotoxic to HT-29 after 24 h incubation with bare-NDs and after 48 h incubation with Au-NDs. Therefore, it is clear that the gold layer increases the biocompatibility of discs despite the uncovered lateral surface of the dots (about 8.5%). Biocompatibility is an important factor to consider when studying an anti-cancer approach characterized by high treatment selectivity thanks to the use of an external stimulus to spatially control the activation of therapeutic nanosystems non-toxic by themselves.

Gold coating provided not only an increased biocompatibility [31] of the NDs but allowed easy surface modification. Thiolate groups can readily react with the gold surface and the preparation of a cysteine-FITC derivative has been exploited to randomly introduce fluorescence on the surface of NDs.

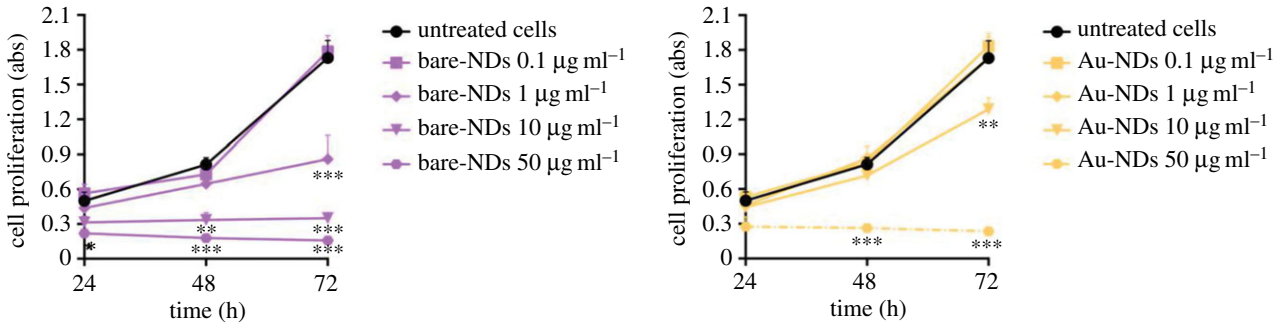

Figure 4. Effects of NDs with and without the protective gold layer on HT-29 cell proliferation. Cell proliferation, after exposure to increasing concentrations of NDs with and without the protective gold layer (0.1, 1, 10 and 50 μg ml^{-1}), has been evaluated at 24, 48 and 72 h by WST-1 assay. Statistical significance versus untreated cells: *$p < 0.05$, **$p < 0.01$, ***$p < 0.001$.

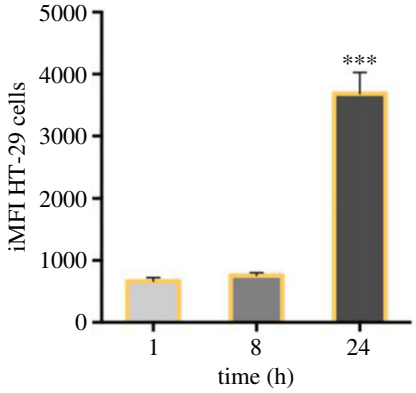

Figure 5. Gold nanodisc cellular uptake. HT-29 cells have been incubated with FITC conjugated gold nanodiscs (Au-NDs) at the same concentration (10 μg ml^{-1}) for 1, 8 and 24 h. Fluorescent signal has been detected using a flow cytometer at 488 nm excitation to measure intracellular NDs and expressed as the iMFI calculated as reported in Material and methods. Statistical significance versus untreated cells: ***$p < 0.001$.

By cytofluorimetric analysis using an FITC conjugate the intracellular uptake of derivatized Au-FITC-NDs has been studied at the highest non-toxic concentration, i.e. 10 μg ml^{-1}. ND cellular uptake significantly increased over time and a significant cellular uptake of Au-NDs has been observed after 24 h incubation, as shown in figure 5. Furthermore, FITC derivatized NDs showed superior dispersion and change in aggregation when compared with the NDs not derivatized.

4. Conclusion

In this work, a self-assembling process based on nanosphere lithography is proposed to fabricate bare and Au-coated $Ni_{80}Fe_{20}$ NDs. Such a parallel process comes out as an easy-to-use, fast and low-cost method to nanostructure thin films. It allows one to fabricate NDs at a higher rate compared with conventional, sequential nanolithography process having a well-defined contour. The magnetization process of all the NDs is characterized by the presence of a vortex pointing to a possible exploitation in drug delivery process and also in magnetic hyperthermia. Finally, cytoxicity text confirms that Au-coated NDs display an improved biocompatibility with respect to the bare ones despite the incomplete coverage of the NDs. The intracellular uptake of the NDs has been confirmed by cytofluorimetric analysis using the FITC conjugate on the surface of Au-coated NDs.

Competing interests. We declare we have no competing interests.
Funding. No funding has been received for this article.

References

1. Pankhurst QA, Connolly J, Jones SK, Dobson J. 2003 Applications of magnetic nanoparticles in biomedicine. *J. Phys. D Appl. Phys.* **36**, R167–R181. (doi:10.1088/0022-3727/36/13/201)
2. Nguyen TKT. 2012 *Magnetic nanoparticles from fabrication to clinical applications*. Boca Raton, FL: CRC Press Taylor & Francis Group.
3. Kang K, Choi J, Nam JH, Lee SC, Kim KJ, Lee S-W, Chang JH. 2009 Preparation and characterization of chemically functionalized silica-coated magnetic nanoparticles as a DNA separator. *J. Phys. Chem. B* **113**, 536–543. (doi:10.1021/jp807081b)
4. Lu C-W *et al.* 2007 Bifunctional magnetic silica nanoparticles for highly efficient human stem cell labeling. *Nano Lett.* **7**, 149–154. (doi:10.1021/nl0624263)
5. Sun C, Lee JSH, Zhang M. 2008 Magnetic nanoparticles in MR imaging and drug delivery. *Adv. Drug Deliv. Rev.* **60**, 1252–1265. (doi:10.1016/j.addr.2008.03.018)
6. Dutz S, Hergt R. 2014 Magnetic particle hyperthermia: a promising tumor therapy? *Nanotechnology* **25**, 452001. (doi:10.1088/0957-4484/25/45/452001)
7. Lu A-H, Salabas EL, Schuth F. 2007 Magnetic nanoparticles: synthesis, protection, functionalization, and application. *Angew. Chem. Int. Edit.* **46**, 1222–1244. (doi:10.1002/anie.200602866)
8. Ito A, Shinkai M, Honda H, Kobayashic T. 2005 Medical application of functionalized magnetic nanoparticles. *J. Biosci. Bioeng.* **100**, 1–11 (doi:10.1263/jbb.100.1)
9. Tamer U, Gundogdu Y, Boyaci IH, Pekmez K. 2009 Synthesis of magnetic core–shell Fe_3O_4–Au nanoparticle for biomolecule immobilization and detection. *J. Nanopart. Res.* **12**, 1187–1196. (doi:10.1007/s11051-009-9749-0)
10. Cho S-J, Idrobo J-C, Olamit J, Liu K, Browning ND, Kauzlarich SM. 2005 Growth mechanisms and oxidation resistance of gold-coated iron nanoparticles. *Chem. Mater.* **17**, 3181–3186. (doi:10.1021/cm0500713)
11. Yu H, Chen M, Rice PM, Wang SX, White RL, Sun S. 2005 Dumbbell-like bifunctional Au–Fe_3O_4 nanoparticles. *Nano Lett.* **5**, 379–382. (doi:10.1021/nl047955q)
12. Wang L, Luo J, Maye MM, Fan Q, Rendeng Q, Engelhard MH, Wang C, Lin Y, Zhong C-J. 2005 Iron

oxide–gold core–shell nanoparticles and thin film assembly. *J. Mater. Chem*. **15**, 1821–1832. (doi:10.1039/B501375E)

13. Caruntu D, Cushing BL, Caruntu G, O'Connor J. 2005 Attachment of gold nanograins onto colloidal magnetite nanocrystals. *Chem. Mater*. **17**, 3398–3402. (doi:10.1021/cm050280n)
14. Tartaj P, del Puerto Morales M, Veintemillas-Verdaguer S, González-Carreño T, Serna CJ. 2003 The preparation of magnetic nanoparticles for applications in biomedicine. *J. Phys. D: Appl. Phys*. **36**, R182–R197. (doi:10.1088/0022-3727/36/13/202)
15. Hasany SF, Ahmed I, Rajan J, Rehman A. 2012 Systematic review of the preparation techniques of iron oxide magnetic nanoparticles. *Nanosci. Nanotechnol*. **2**, 148–158. (doi:10.5923/j.nn.20120206.01)
16. Tiberto P, Barrera G, Celegato F, Conta G, Coïsson M, Vinai F, Albertini F. 2015 $Ni_{80}Fe_{20}$ nanodisks by nanosphere lithography for biomedical applications. *J. Appl. Phys*. **117**, 17B304. (doi:10.1063/1.4913278)
17. Hu W *et al.* 2008 High-moment antiferromagnetic nanoparticles with tunable magnetic properties. *Adv. Mater*. **20**, 1479–1483. (doi:10.1002/adma.200703077)
18. Joisten H, Courcier T, Balint P, Sabon P, Faure-Vincent J, Auffret S, Dieny B. 2010 Self-polarization phenomenon and control of dispersion of synthetic antiferromagnetic nanoparticles for biological applications. *Appl. Phys. Lett*. **97**, 253112. (doi:10.1063/1.3518702)
19. Kosiorek A, Kandulski W, Glaczynska H, Giersig M. 2005 Fabrication of nanoscale rings, dots, and rods by combining shadow nanosphere lithography and annealed polystyrene nanosphere masks. *Small* **1**, 439–444. (doi:10.1002/smll.200400099)
20. Cheng JY, Ross CA, Chan VZ-H, Thomas EL, Lammertink RGH, Vancso GJ. 2001 Formation of a cobalt magnetic dot array via block copolymer lithography. *Adv. Mater*. **13**, 1174–1178. (doi:10.1002/1521-4095(200108)13:15<1174::AID-ADMA1174>3.0.CO;2-Q)
21. Decuzzi P, Ferrari M. 2006 The adhesive strength of non-spherical particles mediated by specific interactions. *Biomaterials* **27**, 5307–5314. (doi:10.1016/j.biomaterials.2006.05.024)
22. Gentile F, Chiappini C, Fine D, Bhavane RC, Peluccio MS, Ming-Cheng Cheng M, Liu X, Ferrari M, Decuzzi P. 2008 The effect of shape on the margination dynamics of non-neutrally buoyant particles in two-dimensional shear flows. *J. Biomech*. **41**, 2312–2318. (doi:10.1016/j.jbiomech.2008.03.021)
23. Decuzzi P, Godin B, Tanaka T, Lee S-Y, Chiappini C, Liu X, Ferrari M. 2010 Size and shape effects in the biodistribution of intravascularly injected particles. *J. Control. Release* **141**, 320–327. (doi:10.1016/j.jconrel.2009.10.014)
24. Coey JMD. 2009 *Magnetism and magnetic materials*. Cambridge, UK: Cambridge University Press.
25. Leulmi S *et al.* 2015 Triggering the apoptosis of targeted human renal cancer cells by the vibration of anisotropic magnetic particles attached to the cell membrane. *Nanoscale* **7**, 15 904–15 914. (doi:10.1039/c5nr03518j)
26. Kim D-H, Rozhkova EA, Ulasov IV, Bader SB, Rajh T, Lesniak MS, Novosad V. 2009 Biofunctionalized magnetic-vortex microdiscs for targeted cancer-cell destruction. *Nat. Mater*. **9**, 165–171. (doi:10.1038/nmat2591)
27. Issa B, Obaidat IM, Albiss BA, Haik Y. 2013 Magnetic nanoparticles: surface effects and properties related to biomedicine applications. *Int. J. Mol. Sci*. **14**, 21 266–21 305. (doi:10.3390/ijms141121266)
28. Chen Y. 2015 Nanofabrication by electron beam lithography and its applications: a review. *Microelectron. Eng*. **135**, 57–72. (doi:10.1016/j.mee.2015.02.042)
29. Weekes SM, Ogrin FY, Murray WA, Keatley PS. 2007 Macroscopic arrays of magnetic nanostructures from self-assembled nanosphere templates. *Langmuir* **23**, 1057–1060. (doi:10.1021/la061396g)
30. Cowburn RP, Koltsov DK, Adeyeye AO, Welland ME, Tricker DM. 1999 Single-domain circular nanomagnets. *Phys. Rev. Lett*. **83**, 1042–1045. (doi:10.1103/PhysRev Lett.83.1042)
31. Nel A, Mädler L, Velegol D, Xia T, Hoek EMV, Somasundaran P, Klaessig F, Castranova V, Thompson M. 2009 Understanding biophysicochemical interactions at the nano–bio interface. *Nat. Mater*. **8**, 543–557. (doi:10.1038/nmat2442)